Density–density correlations in a Luttinger liquid: Lattice approximation in the Calogero–Sutherland model

Diptiman Sen and R.K. Bhaduri

Abstract: For a one-dimensional model in which the two-body interactions are long-range and *strong*, the system almost crystallizes. The harmonic modes of such a lattice were used by Krivnov and Ovchinnikov to compute the ground-state wave function and the dynamical density–density correlations. We review this method, and apply it to the Calogero–Sutherland model, whose density–density correlation functions are exactly known for certain values of the coupling constant. We show numerically that the correlations obtained are quite accurate even if the coupling is not very large. Such comparisons have been made earlier by Forrester. The lattice method is considerably simpler than the ones used to derive the exact results, and yields expressions for the correlations- which are easily plotted. The equal-time correlations can be expanded in inverse powers of coupling; we show that the two leading order terms agree with the exact results which are known for integer values of the coupling. The strength-dependent power law fall-off is typical of a Luttinger liquid. In a general one-dimensional model where the two-body interaction decreases as a power of the relative distance, we argue, following Schulz, that at zero temperature the system behaves as a Luttinger liquid if the power exceeds 1, and as a Wigner crystal if it is less than 1.

PACS Nos.: 63.20-e, 71.10Pm

Résumé: Dans un modèle 1-D où les interactions à deux corps sont de longue portée et *fortes*, le système cristallise presque. Krivnov et Ovchinnikov ont utilisé les modes harmoniques d'un tel réseau pour calculer la fonction d'onde du fondamental et les corrélations dynamiques densité–densité. Nous montrons numériquement que les corrélations ainsi obtenues sont excellentes, même si l'interaction n'est pas très forte. Forrester a déjè effectué ce genre de comparaison. La méthode par réseau est considérablement plus simple que celles utilisées pour obtenir un résultat exact et elle donne des résultats pour les corrélations qui peut facilement être mis en graphique. Les corrélations en temps réel peuvent être développees en série de puissance inverse du couplage ; nous momtrons que les deux premiers termes correspondent au résultat exact pour les valeurs entières du couplage. Cette série, fonction de la force du couplage, a une décroissance de sa loi de puissance qui est typique d'un liquide de Luttinger. Dans un modèle 1-D général, où l'interaction à deux corps decroît comme une puissance de la distance relative, nous soutenons et en accord avec Schulz, qu'à température zéro, le système se comporte comme un liquide de Luttinger si la puissance est >1 et comme un cristal de Wigner si elle est <1. [Traduit par la rédaction]

Received December 10, 1998. Accepted May 19, 1999.

We dedicate this paper to the memory of Heinz Schulz who passed away in November 1998.

D. Sen[1] **and R.K. Bhaduri.** Department of Physics and Astronomy, McMaster University, Hamilton, ON L8S 4M1, Canada.

[1] Permanent address: Centre for Theoretical Studies, Indian Institute of Science, Bangalore 560012, India.

1. Introduction

Quantum many-body systems with strong interactions are usually difficult to analyze. This is particularly true if the system is one-dimensional, in which case the interactions can drastically modify the behavior of its noninteracting counterpart. For example, in such systems, the density–density correlation function, which may be obtained from inelastic scattering experiments, falls off at long distances according to a power that depends smoothly on the strength of the interaction [1,2]. This is one of the characteristic features of a "Luttinger liquid", and it is quite unlike the situation in two or three dimensions where the long-distance power-law is independent of the interaction strength. Clearly, it would be interesting to understand this fundamental property of a large class of one-dimensional quantum systems in a simple way. There is, in fact, an old method of doing this [2]; further, the method works better if the interactions are strong. We apply this method to the Calogero–Sutherland–Moser (CSM) model [3–6], which is actually an ideal Luttinger liquid because the two-body interaction is scale invariant. The Calogero model [3,4] considers N particles on a line interacting mutually with a two-body potential that falls off inversely as the square of the relative distance. In the Sutherland model [5], on the other hand, the particles are on the circumference of a circle, with the two-body interaction being inversely proportional to the square of the length of the chord connecting the two particles. In both models, each particle interacts with all the others, and not just its nearest neighbors. In the thermodynamic limit, the two models have identical bulk properties. For the CSM model, Forrester [7] compared the correlation function calculated by the lattice method with the exact results for some specific values of the interaction strengths. After deriving the expression for the CSM using the lattice method, we present several pictures of the correlation function to illustrate the behavior of a Luttinger liquid. The calculations presented in this review are self-contained, and may be followed by someone with a basic knowledge of quantum mechanics.

The CSM model has received much attention recently owing to its connection with a variety of interesting problems. Some examples are random matrix theory [8,9], quantum spin chains with long-range interactions [10,11], Luttinger liquids [1,12], Gaussian conformal field theories [13], edge states in a quantum Hall system [14], generalized exclusion statistics [15–21], and nonlinear internal waves in a stratified fluid [22]. In particular, recent advances in random matrix theory have related the time-dependent (dynamic) density correlations of the CSM model, for three particular values of the interaction strength, to the response of the spectra of nonintegrable or chaotic quantum systems to arbitrary perturbations. The strength of the perturbation in disordered or chaotic systems plays the same role as the time coordinate in the CSM model [9]. This connection between an integrable model like the CSM and disordered systems is an important development that generalizes the earlier observation [4,8] that the time-independent (static) density correlations of the CSM are related to the eigenvalue distribution of unperturbed nonintegrable Hamiltonians.

Although the quantum mechanical energy spectrum of the CSM has been known for a long time [3,5], its collective properties [23–27] and dynamical density–density correlations [7, 28–32] are not yet expressed in an easily accessible form. The correlations are best understood for three particular values of the coupling parameter $\lambda = 1/2$, 1, and 2, which are closely related to random matrix theory [28,29]. An impressive amount of information is also available for all integer [7,30,31] and rational [32] values of λ. However, even though these are all exact results, the mathematical expressions are not very convenient for plotting, say, the space-time dependence of the correlations, unless λ (or its inverse) is equal to a fairly small integer.

It therefore seems useful to pursue simple and approximate methods for obtaining the correlations for general values of λ. In Sect. 2, we present a method for doing this that is actually exact in the limit of large λ. In that limit, the particles almost freeze into a lattice [11,23]; the harmonic modes about such a lattice may then be used to compute the ground- state energy, wave function, and correlations. We use this idea to obtain the first two terms in an expansion in $1/\lambda$ for the ground-state energy and the asymptotic expression for the equal-time density–density correlation; these agree with the known exact

results [7]. We show that the equal-time correlations given by our method agree reasonably well with the exact result for all distances even if λ is not very large. The dynamical correlations are also obtained with almost equal ease by our method, and are explicitly given for any space-time point. We discuss the low-temperature specific heat, and make a suggestion for improving the correlations by using a slightly modified phonon dispersion. In Sect. 3, we briefly consider a more general model in which the two-body interaction decays as the power α of the distance. We find that the system behaves as a Luttinger liquid if $\alpha > 1$, and as a Wigner crystal if $\alpha < 1$; the Coulomb problem with $\alpha = 1$ lies on the borderline between these two possibilities [33].

2. Calogero–Sutherland–Moser model

We will consider the form of the CSM model in which particles on an infinite line interact pairwise through an inverse-square potential. The model may also be defined on a circle with periodic boundary condition [5]; the two versions of the model have identical physical properties in the thermodynamic limit in which the number of particles N and the length L of the line (or circle) are simultaneously taken to infinity keeping the particle density $\rho_0 = N/L$ fixed. The Hamiltonian for particles on a line is given by

$$H = \sum_n \frac{p_n^2}{2m} + \frac{\hbar^2\lambda(\lambda-1)}{m} \sum_{l<n} \frac{1}{(x_l - x_n)^2} \tag{1}$$

where the dimensionless coupling parameter $\lambda \geq 0$. To make the problem well-defined quantum mechanically, we have to add the condition that the wave functions go to zero as $|x_l - x_n|^\lambda$ whenever two particles l and n approach each other. For $\lambda = 0$ and 1, the model describes free bosons and free fermions, respectively. Since the two-body potential is singular enough to prevent particles from crossing each other, we can choose the wave functions to be either symmetric (bosonic) or antisymmetric (fermionic). The energy spectrum is of course the same in the two descriptions. Two of the exactly known results for this model are as follows [5,23]. In the thermodynamic limit, the ground-state energy E_0 is given by

$$\frac{E_0}{N} = \frac{\pi^2\hbar^2\lambda^2\rho_0^2}{6m} \tag{2}$$

The sound velocity v is given by the group velocity of long-wavelength modes (wavelengths much bigger than the average particle spacing $1/\rho_0$),

$$v = \frac{\pi\hbar\lambda\rho_0}{m} \tag{3}$$

2.1. Ground-state energy and wave function

Let us now consider the limit in which the coupling $\lambda \to \infty$. Then the potential energy term in (1) dominates over the kinetic term. The potential energy is minimized if the particles sit at the sites of a lattice, so that the mean position of the nth particle is $\langle x_n \rangle = n/\rho_0$ [11,23]. The total energy at this order in λ is then given by

$$\frac{E_0}{N} = \frac{\pi^2\hbar^2\lambda(\lambda-1)\rho_0^2}{6m} \tag{4}$$

To the next order in λ, we have to consider the harmonic oscillations about the mean positions. If we denote the fluctuation by $\eta_n = x_n - n/\rho_0$, the Hamiltonian for the phonons is obtained by Taylor

expanding the potential energy in (1) to quadratic order. Thus,

$$H_{ph} = \sum_n \frac{p_n^2}{2m} + \frac{3\hbar^2\lambda(\lambda-1)\rho_0^4}{m} \sum_{l<n} \frac{(\eta_l - \eta_n)^2}{(l-n)^4} \tag{5}$$

where we have ignored higher order anharmonic terms. We now find the dispersion relation ω_q for phonons with wave number q to be

$$\omega_q^2 = \frac{12\hbar^2\lambda(\lambda-1)\rho_0^4}{m^2} \sum_{n=1}^{\infty} \frac{1-\cos(qn/\rho_0)}{n^4} = \frac{\hbar^2\lambda(\lambda-1)}{m^2}\left(\pi\rho_0|q| - \frac{q^2}{2}\right)^2, \qquad |q| \le \pi\rho_0 \tag{6}$$

(Note that q can vary from $-\pi\rho_0$ to $\pi\rho_0$ in steps of $2\pi/L$, so that the total number of modes is N). The sound velocity is given by $v = (\partial\omega_q/\partial q)_{q=0} = \pi\hbar\rho_0\sqrt{\lambda(\lambda-1)}/m$. We see that this agrees with (3) to leading order in λ; we will therefore simply replace $\lambda(\lambda-1)$ by λ^2 in the expression (6) for ω_q^2. Namely, we use the exactly known sound velocity to correct the coefficient of our phonon dispersion. Henceforth we take

$$\omega_q = \frac{\hbar\lambda}{m}\left(\pi\rho_0|q| - \frac{q^2}{2}\right) \tag{7}$$

The zero point energy of the phonons is given by

$$\sum_q \frac{\hbar\omega_q}{2} = L\int_{-\pi\rho_0}^{\pi\rho_0} \frac{dq}{2\pi}\frac{\hbar\omega_q}{2} \tag{8}$$

When this is added to (4), we precisely recover (2); thus the harmonic lattice approximation gives the ground-state energy correctly up to order λ^2 and λ. To get the next order term in the energy, i.e., of order 1, we would have to use the original dispersion (6) as well as consider some of the anharmonic terms beyond H_{ph}; we will not pursue this here.

We now use the harmonic approximation to write down the ground state wave function following ref. 34. The unnormalized wave function for a collection of decoupled phonons is given by

$$\Psi_0 = \exp\left(-\frac{m}{2\hbar}\sum_q \omega_q \eta_q \eta_{-q}\right), \qquad \eta_q = \sum_{n=-\infty}^{\infty} \eta_n e^{iqn/\rho_0} \tag{9}$$

Using the dispersion (7), we find that

$$\Psi_0 = \exp\left(-\frac{\lambda\rho_0^2}{2}\sum_{l<n}\frac{(\eta_l-\eta_n)^2}{(l-n)^2}\right) \tag{10}$$

We see that this is equivalent to the exact ground state wave function of the Hamiltonian (1)

$$\Psi_0 = \prod_{l<n} |\rho_0(x_l - x_n)|^{\lambda} \tag{11}$$

if we Taylor expand

$$\log(\rho_0|x_l - x_n|) = \log|l-n| + \frac{\rho_0(\eta_l-\eta_n)}{l-n} - \frac{\rho_0^2(\eta_l-\eta_n)^2}{2(l-n)^2} + \ldots \tag{12}$$

Before ending this subsection, let us write down the second quantized form for the Heisenberg operators $x_n(t)$,

$$x_n(t) = \frac{n}{\rho_0} + \int_{-\pi\rho_0}^{\pi\rho_0} \frac{\mathrm{d}q}{2\pi} f_q \left[a_q \exp\left[i\left(\frac{qn}{\rho_0} - \omega_q t\right)\right] + a_q^\dagger \exp\left[-i\left(\frac{qn}{\rho_0} - \omega_q t\right)\right]\right]$$

$$f_q = \left(\frac{\hbar}{2m\rho_0\omega_q}\right)^{1/2} \tag{13}$$

Here

$$[a_q, a_{q'}^\dagger] = 2\pi\delta(q - q') \tag{14}$$

We can verify that $p_n(t) = m\,\mathrm{d}x_n(t)/\mathrm{d}t$ satisfies the equal-time commutation relation $[x_l, p_n] = i\hbar\delta_{ln}$.

2.2. Dynamical-correlation function

We now use the harmonic lattice approximation to derive the dynamical density–density correlations defined as [35]

$$g(x, t) = \langle 0|\rho(x, t)\rho(0, 0)|0\rangle, \qquad \rho(x, t) = \sum_n \delta(x - x_n(t)) \tag{15}$$

where $x_n(t)$ is the Heisenberg operator given in (13). To compute this, we write the δ-functions in (15) as

$$\delta(x - x_n(t)) = \int_{-\infty}^{\infty} \frac{\mathrm{d}q}{2\pi}\, \mathrm{e}^{iq(x - x_n(t))} \tag{16}$$

We then evaluate expectation values of the form $\langle 0|\exp[-i(qx_n(t) + q'x_l(0))]|0\rangle$ using the Baker–Campbell–Hausdorff formula [36],

$$\mathrm{e}^{A+B} = \mathrm{e}^A\,\mathrm{e}^B\,\mathrm{e}^{[B,A]/2} \tag{17}$$

if $[B, A]$ commutes with both A and B. We have to evaluate

$$g(x, t) = \int_{-\infty}^{\infty}\int_{-\infty}^{\infty} \frac{\mathrm{d}q}{2\pi}\frac{\mathrm{d}q'}{2\pi} \sum_{n,l} \langle 0|\,\mathrm{e}^{iq(x - x_n(t))}\,\mathrm{e}^{-iq'x_l(0)}|0\rangle \tag{18}$$

On simplifying this using (13) and (17), we find a term like

$$\exp\left[-\frac{1}{2}(q + q')^2 \int_{-\pi\rho_0}^{\pi\rho_0} \frac{\mathrm{d}k}{2\pi} f_k^2\right] \tag{19}$$

Since the integral has a logarithmic divergence at small values of k of the type $\int \mathrm{d}k/\omega_k$, the exponential vanishes unless $q = -q'$. We thus get a δ-function of the form $\delta_{q,-q'} = (2\pi/L)\delta(q + q')$ in the continuum limit. Next, the expectation value in (18) only depends on the coordinate difference $n - l$, not on n and l separately. We can therefore extract a sum $\sum_l 1 = N$; this gives rise to a factor of $\rho_0 = N/L$. Putting everything together, we get

$$g(x, t) = \rho_0 \int_{-\infty}^{\infty} \frac{\mathrm{d}q}{2\pi} \sum_{n=-\infty}^{\infty} \exp\left[iq\left(x - \frac{n}{\rho_0}\right) - \frac{q^2}{\rho_0^2} F(n, t)\right] \tag{20}$$

Fig. 1. Equal-time correlation $g(x)/\rho_0^2$ for $\lambda = 2$. The continuous and dotted lines denote the exact result and the lattice approximation, respectively.

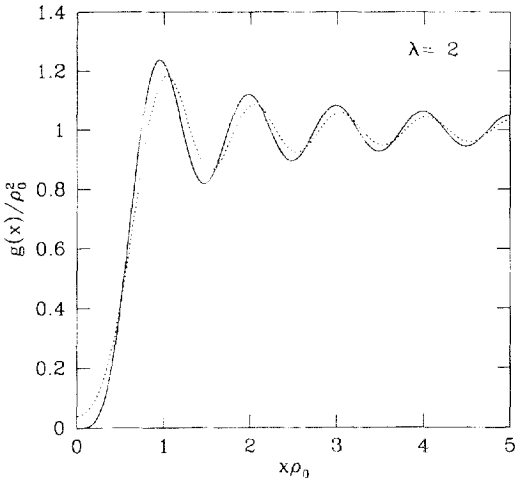

Fig. 2. Correlation $g(x)/\rho_0^2$ for $\lambda = 4$ obtained by the lattice approximation.

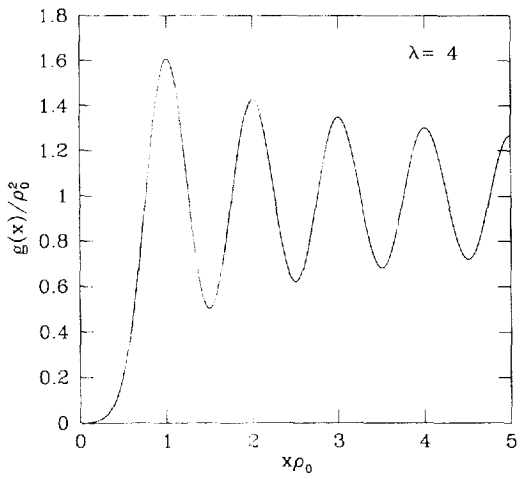

where

$$F(n,t) = \int_0^{\pi\rho_0} \frac{dk}{\pi} \frac{h\rho_0}{2m\omega_k} \left[1 - e^{-i\omega_k t} \cos\left(\frac{kn}{\rho_0}\right)\right] \tag{21}$$

It can be shown that the real part of $F(n,t)$ is always positive, unless both n and t are zero. We can therefore perform the q integration in (20) to get

$$g(x,t) = \rho_0^2 \sum_{n=-\infty}^{\infty} \left(\frac{1}{4\pi F(n,t)}\right)^{1/2} \exp\left[-\frac{(x\rho_0 - n)^2}{4F(n,t)}\right] \tag{22}$$

The expansion in (20) can be understood in a physically intuitive way as follows. Each lattice point n contributes a Gaussian (correctly normalized to unity) to $g(x,t)$: the squared width of the Gaussian is given by the mean square fluctuation

$$\frac{2F(n,t)}{\rho_0^2} = \langle 0|\left(x_n(t) - x_0(0) - \frac{n}{\rho_0}\right)^2 |0\rangle \tag{23}$$

Let us now study the equal-time correlations $g(x,0) \equiv g(x)$ in some detail. From (21), we see that $F(n,0)$ is purely real, and $F(0,0) = 0$. We therefore obtain

$$g(x) = \rho_0 \delta(x) + \rho_0^2 \sum_{n\neq 0} \left(\frac{1}{4\pi F(n,0)}\right)^{1/2} \exp\left[-\frac{(x\rho_0 - n)^2}{4F(n,0)}\right] \tag{24}$$

where

$$\lambda F(n,0) = \frac{1}{2\pi^2} \int_0^{\pi} dy \frac{1 - \cos(yn)}{y - y^2/2\pi} = \frac{1}{2\pi^2} \int_0^{2\pi} dy \frac{1 - \cos(yn)}{y} \tag{25}$$

This gives us [37]

$$\lambda F(n,0) = \frac{1}{2\pi^2}\left[\log\ (2\pi\, e^{\gamma} n) - \mathrm{Ci}(2\pi n)\right] \tag{26}$$

Fig. 3. Static form factor $S(q)/\rho_0$ for $\lambda = 2$. The continuous and dotted lines denote the exact result and the lattice approximation, respectively.

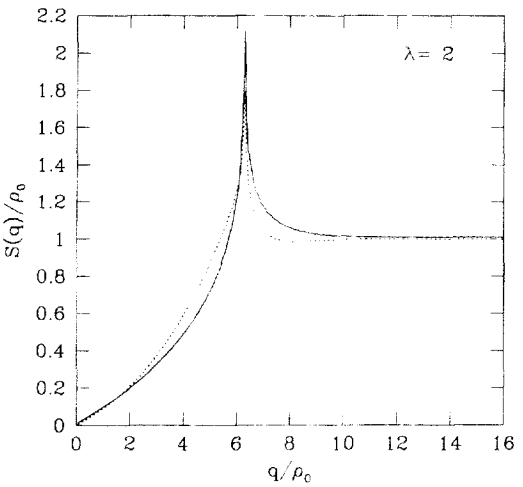

Fig. 4. $S(q)/\rho_0$ for $\lambda = 4$ obtained by the lattice approximation.

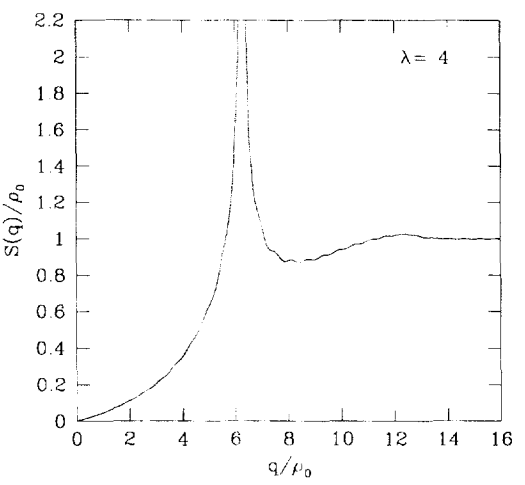

where $\gamma \simeq 0.577\,22$ is Euler's constant, and Ci denotes the cosine integral. For large integer n, (26) has an asymptotic expansion beginning as

$$\lambda F(n,0) = \frac{1}{2\pi^2}\log(Cn) + \frac{1}{8\pi^4 n^2} + O\left(\frac{1}{n^4}\right) \tag{27}$$

where

$$C = 2\pi\, e^{\gamma} \simeq 11.191 \tag{28}$$

The expansion in (27) converges extremely rapidly; for $n = 1$ and 2, the difference between (26) and the first two terms in (27) is only about 0.1% and 0.01%, respectively. For numerical purposes, therefore, we will use (27) to compute $g(x)$ from (24).

We show a plot of $g(x)/\rho_0^2$ vs. $x\rho_0$ for $\lambda = 2$ in Fig. 1; the continuous line denotes the exact result [5], while the dotted line shows our lattice approximation (24). The agreement appears to be reasonable even though λ is not very large; for instance, the root-mean-square fluctuation for nearest-neighbor particles is given by (23) and (27) to be $\sqrt{0.247/\lambda}/\rho_0$, which is as large as 35% of the lattice spacing $1/\rho_0$ for $\lambda = 2$. In Fig. 2, we show the lattice approximation for $g(x)/\rho_0^2$ for $\lambda = 4$. It is clear that the system shows an increasing tendency to crystallize as λ increases. We should note that the δ-function at the origin has not been shown in Figs. 1 and 2; thus the $g(x)$ shown in the figures integrates to one hole.

$$\lim_{n\to\infty} 2\int_0^{n/2} dx\, g(x) = \rho_0(n-1) \tag{29}$$

We also note that in the lattice approximation, $g(x)$ does not quite vanish at $x = 0$ as it should in an exact calculation; however $g(0)$ does become rapidly smaller as λ increases.

We can Fourier transform $g(x)$ to obtain the static form factor

$$S(q) = \int_{-\infty}^{\infty} dx\, e^{-iqx}\, g(x) \tag{30}$$

Since $g(x) \to 1$ for large x, $S(q)$ has a δ-function at the origin. Hence, it is easier to compute

$$S(q) - 2\pi\rho_0^2\delta(q) = \rho_0 + \rho_0^2 \int_0^\infty dx \cos(qx)\left[\sum_{n\neq 0} \frac{\exp\left[-\frac{(x\rho_0-n)^2}{4F(n,0)}\right]}{\sqrt{\pi F(n,0)}} - 2\right] \tag{31}$$

We show a plot of $S(q)/\rho_0$ vs. q/ρ_0 in Fig. 3 for $\lambda = 2$ (the continuous and dotted lines again denote the exact result and the lattice approximation, respectively), and in Fig. 4 for $\lambda = 4$. We will comment on the divergences at $q/\rho_0 = 2\pi$ in subsection C. (The small wiggles in Fig. 4 are due to numerical inaccuracies: the integral in (31) converges very slowly if λ is large. The power-law that governs the convergence will also be derived in the next subsection).

We now consider the dynamical correlations $g(x, t)$. It is convenient to introduce a dimensionless time variable

$$\tilde{t} = vt\rho_0 \tag{32}$$

Then

$$\lambda F(n,t) = \frac{1}{2\pi^2}\int_0^\pi dy \frac{1-\cos(yn)\exp\left[-i\tilde{t}(y-y^2/2\pi)\right]}{y-y^2/2\pi} \tag{33}$$

In the lattice approximation, plotting $g(x, t)$ is almost as easy as plotting $g(x)$. In Figs. 5 and 6, we show $g(x, t)/\rho_0^2$ vs. $x\rho_0$ for $\tilde{t} = 0.2$ and $\tilde{t} = 2$, respectively, both for $\lambda = 2$. The continuous and dotted lines show the real and imaginary parts, respectively. Note that the δ-function at the origin, which was not shown for $g(x)$ in Fig. 1, has now spread out and become visible at finite time in Figs. 5 and 6; hence there is no hole in the real part of $g(x, t)$. For a small value of time $\tilde{t}$ and for x close to the origin (Fig. 5), the δ-function at the origin spreads out as a free particle with dispersion $\omega_q = \hbar q^2/2m$; this explains the large oscillations in both the real and imaginary parts. For a larger value of time (Fig. 6), and also for larger values of x for any time, the particle feels the harmonic force of the lattice. Hence the behavior of $g(x, t)$ is different from the spreading of a free particle; in particular, the large oscillations get damped out. Finally, note that for $\tilde{t} = 2$, $g(x, t)$ can differ appreciably from $g(x, 0)$ only in the region $x\rho_0 = 0$ to 2, since phonons can only propagate that far in that time. This is most strikingly visible in Fig. 5 in the imaginary part of $g(x, t)$ which vanishes rapidly beyond $x\rho_0 = 2$.

Given $g(x, t)$, we can Fourier transform the x coordinate to obtain a function which we denote by

$$S(q,t) = \rho_0 \sum_{n=-\infty}^{\infty} \exp\left[-\frac{iqn}{\rho_0} - \frac{q^2}{\rho_0^2}F(n,t)\right] \tag{34}$$

Thus the function $S(q)$ given in (30) is equal to $S(q, t = 0)$. If we now Fourier transform (34) in time, we obtain the dynamical structure factor

$$S(q,\omega) = \int_{-\infty}^{\infty} dt\, e^{i\omega t}\, S(q,t) \tag{35}$$

This quantity can be written in terms of all the excited states $|v\rangle$ of the system,

$$S(q,\omega) = \rho_0 \sum_{v\neq 0} 2\pi\delta(\omega - E_v + E_0)|\langle v|\rho(q)|0\rangle|^2, \qquad \rho(q) = \int dx \rho(x) e^{-iqx} = \sum_n e^{-iqx_n} \tag{36}$$

It is useful to consider the moments of $S(q, \omega)$ [28]

$$I_n(q) = \int_{-\infty}^{\infty} \frac{d\omega}{2\pi}\omega^n\, S(q,\omega) \tag{37}$$

Fig. 5. Dynamical correlation $g(x,t)/\rho_0^2$ for $\lambda = 2$ and $vt\rho_0 = 0.2$ obtained by the lattice approximation. The continuous and dotted lines denote the real and imaginary parts, respectively.

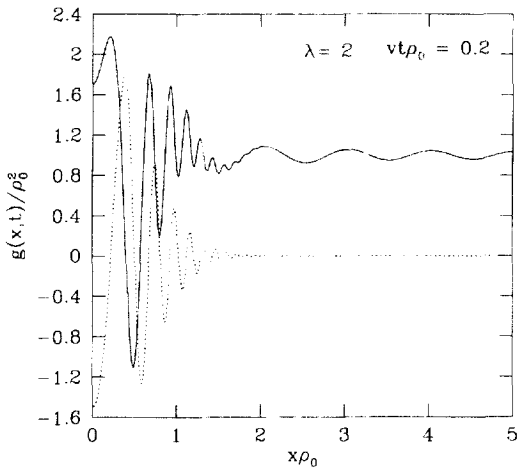

Fig. 6. Correlation $g(x,t)/\rho_0^2$ for $\lambda = 2$ and $vt\rho_0 = 2$ obtained by the lattice approximation. The continuous and dotted lines denote the real and imaginary parts, respectively.

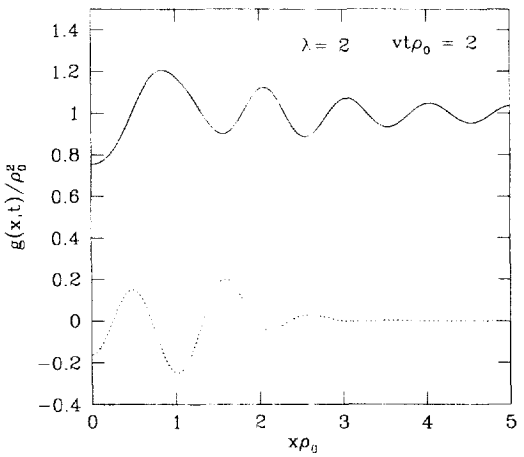

These can be numerically obtained in a straightforward way from (34), since

$$I_n(q) = i^n(\partial^n S(q,t)/\partial t^n)_{t=0}$$

We have already considered $I_0(q) = S(q)$ above. Since

$$F(0,0) = 0$$

and

$$(\partial F(n,t)/\partial t)_{t=0} = i\delta_{n,0}\,\hbar\rho_0^2/2m$$

we find that the first moment

$$I_1(q) = \frac{\hbar q^2 \rho_0}{2m} \tag{38}$$

is independent of λ. This is an exact result following from the velocity independence of the two-body interactions, and it is called the f-sum rule. The second moment $I_2(q)$ is shown in Fig. 7 for $\lambda = 2$; we have actually plotted $I_2(q)m^2/(\hbar^2\rho_0^2 q^3)$ which is dimensionless and has a constant limit at $q = 0$.

At this point, we observe the phenomenon of saturation by sound modes for small momenta [28]. Namely, for $q << 2\pi\rho_0$, $S(q,\omega)$ is dominated by values of ω close to the phonon energy ω_q given by (7); thus $I_n(q)/I_0(q)$ approaches ω_q^n as $q \to 0$. Hence, the y-coordinate in Fig. 7 should approach $\pi\lambda/2$ at $q = 0$ which it does. For the same reason, the curves in Figs. 3 and 4 are linear near the origin with a slope of $1/(2\pi\lambda)$, since $S(q)\rho_0$ approaches $\hbar q^2/(2m\omega_q)$.

The saturation by phonons at low energies also has a bearing on low-temperature thermodynamic properties of the CSM model like the specific heat and pressure. We use the dispersion (7) to compute the free energy per unit length f taking the phonons to have zero chemical potential. Thus,

$$\beta f = \int_{-\infty}^{\infty} \frac{dq}{2\pi} \ln\left(1 - e^{-\beta\hbar\omega_q}\right) \tag{39}$$

Fig. 7. Second moment of dynamical structure factor $I_2(q)m^2/(\hbar^2\rho_0^2q^3)$ for $\lambda = 2$ obtained by the lattice approximation.

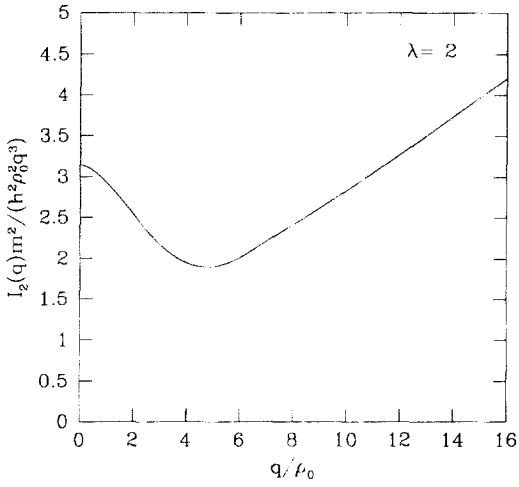

Fig. 8. Equal-time correlation $g(x)/\rho_0^2$ for $\lambda = 2$. The continuous and dotted lines denote the exact result and the lattice approximation using the modified dispersion relation (41), respectively.

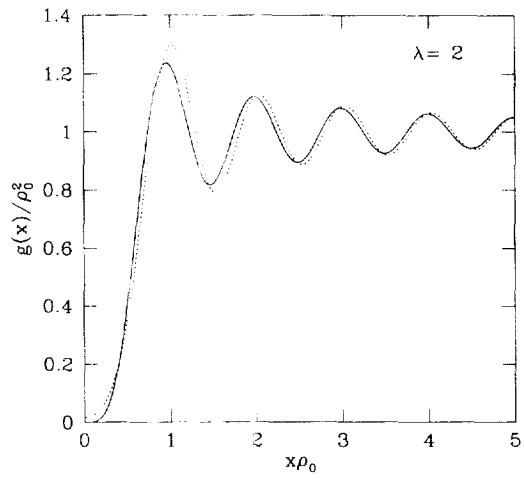

where $\beta = 1/k_BT$. After evaluating this, we obtain the specific heat per unit length $C_V = -T\partial^2 f/\partial T^2$ to second order in T. We find

$$C_V = \frac{\pi k_B^2 T}{3\hbar v} + \frac{6\zeta(3)\lambda}{\pi}\frac{k_B^3 T^2}{\hbar m v^3}, \qquad \zeta(3) = \sum_{n=1}^{\infty}\frac{1}{n^3} \simeq 1.2021 \tag{40}$$

On comparing this with the exact result in ref. 20, we see that we have the correct coefficient for the term of order T; this is related to having the right phonon velocity at $q = 0$. However, we have a coefficient λ instead of $\lambda - 1$ for the term of order T^2 in (40). A different approach to the CSM based on collective field theory actually gives a dispersion [27]

$$\omega_q = \frac{\hbar}{m}\left(\pi\rho_0\lambda\,|q| - (\lambda - 1)\frac{q^2}{2}\right) \tag{41}$$

which leads to the correct coefficient $\lambda - 1$ for the T^2 term. All this suggests that we may get more accurate low-momentum or long-distance correlations if we use the dispersion (41) instead of (7). Let us therefore use (41) to compute $F(n, 0)$ and then $g(x, 0)$ following (21) and (22). The result is plotted and compared with the exact results for $\lambda = 2$ in Fig. 8. On contrasting this with Fig. 1, which is based on the dispersion (7), we see an improved agreement for large values of x, and, somewhat unexpectedly, for very small x also. This analysis again shows the close connection between the phonon dispersion and the correlations in the lattice formalism.

2.3. Large-x asymptotics for $g(x)$

We will now analytically evaluate $g(x)$ in (24) for large values of x, and show that the order 1 and $1/\lambda$ terms agree with the exact results given in ref. 7. We use the Poisson resummation formula [38]

$$\sum_{n=-\infty}^{\infty}\phi(n) = \sum_{p=-\infty}^{\infty}\int_{-\infty}^{\infty} dy\, e^{i2\pi yp}\,\phi(y) \tag{42}$$

Given a function $\phi(n)$ defined for integer values, there are clearly many ways to interpolate it to a function of a real variable $\phi(y)$. Equation (42) says that different interpolations on the right-hand side (assuming that the integrals and sum converge) must give the same answer for the left-hand side. We will use this freedom to interpolate $F(n, 0)$ to $F(y, 0)$ taking the function in (27), rather than the one in (26). This is a convenient choice because the function in (27) is smooth, unlike (26) which contains oscillations. Thus, we use (42) with

$$\phi(y) = \left(\frac{\lambda}{4\pi f(y)}\right)^{1/2} \exp\left[-\frac{\lambda(y - x\rho_0)^2}{4f(y)}\right] \tag{43}$$

where $f(y)$ and its first two derivatives have the form

$$f(y) = \frac{1}{2\pi^2}\log(Cy) + \frac{1}{8\pi^4 y^2} + O\left(\frac{1}{y^4}\right)$$

$$f'(y) = \frac{1}{2\pi^2 y} - \frac{1}{4\pi^4 y^3} + O\left(\frac{1}{y^5}\right)$$

$$f''(y) = -\frac{1}{2\pi^2 y^2} + \frac{3}{4\pi^4 y^4} + O\left(\frac{1}{y^6}\right) \tag{44}$$

We now Taylor expand $\phi(y)$ around $y = x\rho_0$, and do the integrals over y on the right-hand side of (42). Up to order $1/\lambda$, this yields the general expression

$$\frac{g(x)}{\rho_0^2} = 1 + \frac{f''(x)}{\lambda} + 2\sum_{p=1}^{\infty} \exp\left(-\frac{4\pi^2 p^2 f(x)}{\lambda}\right)\left[\left(1 + \frac{f''(x)}{\lambda}\right)\cos(2\pi p x) - \frac{4\pi p f'(x)}{\lambda}\sin(2\pi p x)\right] \tag{45}$$

We now use the explicit forms for $f(y)$ and its derivatives in (44) to obtain, up to order $1/x^2$,

$$\frac{g(x)}{\rho_0^2} = 1 - \frac{1}{2\lambda\pi^2 x^2} + 2\sum_{p=1}^{\infty} (Cx\, e^{1/4\pi^2 x^2})^{-2p^2/\lambda}\left[\left(1 - \frac{1}{2\lambda\pi^2 x^2}\right)\cos(2\pi p x) - \frac{2p}{\lambda\pi x}\sin(2\pi p x)\right] \tag{46}$$

(On the right-hand sides of (45-46), we have written x instead of $x\rho_0$ for convenience). Equation (46) agrees with the asymptotic expression given in ref. 7 up to $O(\frac{1}{\lambda}, \frac{1}{x^3})$. We should make two comments here. First, the sum over p runs to infinity in (46), while it stops at $p = \lambda$ in the exact result for integer λ; however, the difference between the two is exponentially small for large λ. Secondly, by going up to order $1/\lambda^2$, we find terms involving $\log x$ which are not present in the exact result. This shows that the harmonic lattice approximation fails at order $1/\lambda^2$, and that anharmonic terms must be included to recover the correct asymptotics at that order.

The oscillatory terms in (46) imply that the Fourier transform $S(q)$ diverges at momenta $q = 2\pi p\rho_0$ for all nonzero integers p satisfying $p^2 \leq \lambda/2$. The divergence has a power-law form $|q -$

$2\pi p\rho_0|^{(2p^2/\lambda)-1}$ if $p^2 < \lambda/2$, and is logarithmic if $p^2 = \lambda/2$. We indeed see a logarithmic divergence in Fig. 3 for $\lambda = 2$, and a square-root divergence in Fig. 4 for $\lambda = 4$, both at $q = 2\pi\rho_0$.

The asymptotic analysis can be extended to the dynamical correlations $g(x,t)$. Let us define

$$s = \rho_0 |x^2 - v^2t^2|^{1/2} \tag{47}$$

and assume that $s >> 1$. Then we can show that the leading term in (21) is given by

$$F(n,t) = \frac{1}{2\pi^2\lambda} \log (Cs) \tag{48}$$

Following the above arguments, we find that

$$g(x,t) = \rho_0^2 \left[1 + 2 \sum_{p=1}^{\infty} (Cs)^{-2p^2/\lambda} \cos(2\pi x p\rho_0) \right] \tag{49}$$

to leading order in the $1/\lambda$ expansion.

The various power-law exponents derived above are in accordance with arguments based on the idea of Luttinger liquids and conformal field theory [1,13,39]. In general, if the phonons in a one-dimensional system have a low-momentum dispersion of the form $\omega_q \simeq vq$, the arguments presented here show that the prefactors of the oscillatory terms in (45) must decay with the exponents $2\pi h\rho_0 p^2/(mv)$. In the next section, we will study the conditions under which a class of long-range interactions can lead to Luttinger liquidlike behavior.

2.4. Other Long-range models

We consider a one-dimensional system in which the two-body interactions decay as the power α of the distance. Using the lattice approximation, we find that the long-distance correlations are quite different depending on whether $\alpha > 1$, $\alpha = 1$ (the Coulomb problem), or $0 < \alpha < 1$ [33]. This follows directly from the phonon dispersion, which has the form

$$\omega_q^2 \sim \sum_{n=1}^{\infty} \frac{1 - \cos(qn)}{n^{\alpha+2}} \tag{50}$$

(We set the density $\rho_0 = 1$ in this section). For low momenta, $q << \pi$, we see that

$$\omega_q \sim |q| \quad \text{if} \quad \alpha > 1$$

$$\omega_q \sim |q| \sqrt{\log |q|} \quad \text{if} \quad \alpha = 1$$

$$\omega_q \sim |q|^{(\alpha+1)/2} \quad \text{if} \quad 0 < \alpha < 1 \tag{51}$$

The asymptotics of the correlations $g(x)$ are governed by the long-distance behavior of

$$F(n) \sim \int_0^{\pi} \frac{dq}{\omega_q} \left[1 - \cos(qn) \right] \tag{52}$$

This diverges as $\log n$ if $\alpha > 1$ and as $\sqrt{\log n}$ if $\alpha = 1$, but it does not diverge if $\alpha < 1$. Correspondingly, the prefactors of the oscillatory terms in $g(x)$ decay as powers of x if $\alpha > 1$ (Luttinger liquid) and as exponentials of $-\sqrt{\log x}$ if $\alpha = 1$, but they do not decay if $\alpha < 1$ (Wigner crystal) [33]. It is amusing that the Coulomb system, which is physically the most interesting of the three cases, lies exactly in between the Luttinger liquid and Wigner crystal scenarios.

3. Discussion

We have seen that the harmonic lattice approximation is an useful technique from which many properties of the CSM can be derived readily without having to solve the Schrödinger equation (1) in great detail. It is remarkable that the results obtained are numerically quite accurate even if λ is not very large, and the mean square fluctuation of each particle from its average position is not much smaller than the lattice spacing. An interesting problem for future study may be to go systematically to higher orders in the $1/\lambda$ expansion by starting from the original phonon dispersion (6) and include the anharmonic terms perturbatively. This may provide a justification for replacing the dispersion (6) by either (7) or (41), and may enable us to extend our results to smaller values of λ.

It may be worth pointing out that although the lattice method begins by assuming a crystalline configuration for the particles, a genuine crystal which spontaneously breaks the translation invariance of the Hamiltonian does not exist in one dimension even at zero temperature. Thus, if we compute the expectation value $\langle 0|\rho(x)|0\rangle$, we find that it is equal to ρ_0 for all x. This happens because the integral $\int \mathrm{d}k/\omega_k$ diverges logarithmically near $k = 0$, so that $\langle 0|\rho(k)|0\rangle$ vanishes unless the momentum $k = 0$. We therefore see that the harmonic fluctuations in the crystalline ansatz actually restore translation invariance in the ground state.

Before ending, we would like to mention some examples of Luttinger liquids in one dimension where the results of this paper may possibly have some applications [39]. The long-distance and low-energy properties of Luttinger liquids are determined by *two* parameters, namely, the velocity v and the interaction strength λ. Both of these depend on the various parameters which govern the microscopic Hamiltonian of the system. Three examples of systems which behave as Luttinger liquids are quantum spin chains (including some spin ladders), quantum wires, and edge states in a fractional quantum Hall system. Antiferromagnetic spin-1/2 chains have a long history going back to their exact solution by the Bethe ansatz. In recent years, many experimental systems have been studied which are well-described by quasi-one-dimensional half-odd-integer spin models with isotropic (Heisenberg) interactions. Such systems are known to behave like a Luttinger liquid with $\lambda = 2$. It seems to be difficult to vary λ experimentally in spin systems. In contrast, a single-channel quantum wire (which is basically a system of interacting electrons which are geometrically constrained to move along one particular direction) typically has two low-energy sectors, both of which are Luttinger liquids (except for special densities like half-filling). One of these is the spin sector which again has $\lambda = 2$; this value of λ is special because a Luttinger liquid has an $SU(2)$ symmetry at that value. The other one is the charge sector whose λ value depends on a smooth way on the different interactions present in the system. Finally, the edge states in a fractional quantum Hall system behave as a Luttinger liquid with λ taking certain discrete rational values; the value of λ can be changed by altering the electron density and the magnetic field in the bulk of the system. For all these systems, many properties have been measured such as the response to external electric and magnetic fields (conductivity or susceptibility) and to disorder, scattering of neutrons or photons from these systems and specific heat. These measurements clearly indicate the Luttinger liquid-like behavior of these systems with various critical exponents depending in a non-universal way on the interactions in the system. However, it is difficult to directly apply the results in this paper to these experimental systems because they are not *ideal* Luttinger liquids; they exhibit corrections (such as logarithms of distances or temperatures) due to the presence of other terms, such as various short-range interactions which introduce additional length scales into the problem, or the interactions in the transverse directions which violate the one-dimensionality. These corrections make it difficult to extract the two Luttinger parameters from the experimental data.

Acknowledgements

DS thanks F. D. M. Haldane for a stimulating discussion, and the Department of Physics and Astronomy, McMaster University for its hospitality during the course of this work. The authors are grateful to Don

Sprung tor going through the manuscript carefully This research was supported by the Natural Science\ and Engineering Research Council of Canada

References

1. F.D.M. Haldane. Phys. Rev. Lett. **47.** 1840 (1981); **45**. 1358 (1981).
2. V.Ya. Krivnov and A.A. Ovchinnikov. **Sov.** Phys. JETP **55.** 162 (1982); A V Zahrodin and A.A. Ovchinnikov. Sov. Phys. JETP **63,** 1326 (1986).
3. F. Calogero. J. Math. Phys. **10.** 2191 (1969); **10,2197** (1969).
4. B. Sutherland. J. Math. Phys. **12,** 246 (1971); **12**. 251 **(1971).**
5. B. Sutherland. Phys. Rev. A: Gen. Phys. **4.** 2019 (1971); **5**. 1372 (1972); Phys. Rev. B: Condens. Matter. **45**, **907** (1992).
6. J. Moser. Adv. Math. **16,** 197 (1975); F. Calogero. Lett. Nuovo Cimento. 13.411 (1975); A.P. Polychronakos. Phys. Rev. Lett. **69**. 703 (1992).
7. P.J. Forrecter. Phys. Lett. A: At. Mol. Opt. Phys. **179,** 127 (1993); Nucl. Phys. **B388**, 671 (1992); J. Stat. Phys. **72,** 39 **i**1993).
8. M.L. Mehta. Random matrices. Academic Press. New York. 1991.
9. B.D. Simons. P.A. Lee, and B.L. Altshuler. Phys. Rev. Lett. **72,** 64 (1994); B.S. Shastry. *In* Proceedings **of** the 16th Taniguchi Symposium on Correlation Effects in Low Dimensional Electron Effects. Shima, Japan. October,1993. *Edited by* A. Okiji and N. Kauakami. Springer. Berlin. 1994: S. Iain. Mod. Phys. Lett. A, **11.** 1201 (1996).
10. F.D.M. Haldane. Phys. Rev. Lett **60.** 635 (1988); B.S. Shastry. Phys Rev. Lett. **60.** 639 (1988).
11. A.P. Polychronahos. Phys. Rev. Lett. **70.** 2329 (1993); Nucl. Phys. **B419**. *553* (1994).
12. K. Schönhammer and V. Meden. Am. J. Phys **64**. 1168 (1996).
13. N. Kawakami and S.-K. Yang. Phys. Rev. Lett. **67,** 2493 (1991); A.G Izergin, V.E. Korepin, and N.Yu. Reshetikhin. J. Phys. **A:** Math. Gen. **22,** 2615 (1989); T. Fukui and N. Kawakami. Phys. Rev. B: Condens. Matter, **51,** 5239 (1995); J. Phys A: Math. Gen. **28. 6027** (1995).
14. N. Kawakami. Phys. Rev. Lett. **71**, **275** (1993); Y. Yu and Z. Zhu. Commun Theor. Phys. **29,** 351 (1998).
15. F.D.M. Haldane Phys. Rev. Lett **67.937** (1991).
16. M.V.N. Murthy and R. Shankar. Phys. Rev. I ett. **72,** 3629 (1994); **73.** 3331 (1994).
17. A. Dasnieres de Veigy and **S.** Ouvry. Phys. Rev. Lett. **72.** 600 (1994); Mod. Phys. Lett. A. **10**. 1 (1995).
18. Y.-S. Wu. Phys. Rev. Lett. **73.** 922 (1994):D. Bernard and Y.-S. Wu. *In* Proceedings of the 6th Nankai workshop on New developments of integrable systems and long-ranged interaction models. *Edited by* M. L. Ge and Y-S. Wu World Scientific, Singapore. 1995.
19. S.B. Isakov. Phys. Rev. Lett. **73.** 2150 (1994); Int. J. Mod. Phys. A, **9**. 2563 (1994); Mod. Phys. Lett. B. **8.** 319 (1994).
20. S.B. Isakov, D.P. Arovas. J. Myrheim, and A.P. Polychronakos. Phys Lett. **212A.** 29Y (1996); C. Nayak and F. Wilczek. Phys. Rev. Lett. **73, 1710** (1994).
21. D. Sen and R. K Bhaduri. Phys Rev. Lett. **74**, 3912 (1995).
22. H.H. Chen, Y.C Lee. and N.R. Pereira. Phys Fluids. **22.** 187 (1979).
23. B. Sutherland and J. Campbell. Phys. Rev. B: Condens. Matter, **50,** 888 (1994)
24. A.P. Polychronakos. Phys. Rev. Lett. **74.** 5153 (1995).
25. I. Andrić. V. Bardek, and L. Jonke. Phys. Lett. **357B**. **374** (1995); J. Phys. A: Math. Gen. **30.** 717 (1997).
26. I. Andrić and V Bardek. J. Phys. A: Math. Gen. **21. 1847** (1988); I. Andrić. A. Jevicki, and H. Levine. Nucl. Phys. **B215**. 307 (1983).
27. D. Sen and R.K. Bhaduri. Ann. Phys. (NY). **260.203** (1997).
28. E.R. Mucciolo, B.S. Shastry, B.D. Simons. and B.L. Altshuler. Phys Rev. B: Condens. Matter. **49,** 15197 (1994).
29. M.R. Zirnbauer and F.D M. Haldane. Phys. Rev. B: Condens. Matter. **52**. 8729 (1995).
30. J.A. Minahan and A.P. Polychronakos. Phys. Rev. B: Condens. Matter. **50**. 4236 (1994).
31. D. Serban. F. Lesage, and V. Pasquier. Nucl. Phys. **B466.499** (1996); F Lesage, V. Pasquier. and D. Serhan. Nucl. Phys. **B435**, 585 (1995).
32. Z.N.C. Ha. Nucl. Phys. **B435**, 604 (1995).
33. H.J. Schulz. Phys. Rev. Lett. **71,** 1864 (1993).

34. L. Reatto and G.V. Chester Phys. Rev. **155.** 88 (1967).
35. **A.** Ishihara. Condensed matter physics. Oxford University Press. Oxford. 199'
36. E. Merzbacher. Quantum mechanics. John Wiley, New York. 1970. p. 167
37. M. Abramowitz and I.A Stegun. Handbook of mathematical functions Publications. New York. 1972. pp. 231-233.
38. H. Kleinert. Path integrals in quantum statistics arid polymer physics. Scientific. Singapore. 1990. p. 116.
39. H.J. Schulz, G Cuniberti, and P. Pieri. Lecture Notes of the Chia Laguna Summer School **H.J.**Schulz. it In Proceedings of Les Houches Summer School LXI. *Edited b*\ E. Akkermans. G. Montamhaux. J. Pichard, **J.** Zinn-Justin. Elsevier. Amsterdam, 1995. http://xxu.lanl.p\/abs/cond-mat/95031SO.